Microstructural development during the quenching and partitioning process in a newly designed low-carbon steel

Santofimia Navarro, MJ; Zhao, L; Petrov, RH; Kwakernaak, C; Sloof, WG; Sietsma, J

DOI
10.1016/j.actamat.2011.06.014

Publication date
2011

Document Version
Final published version

Published in
Acta Materialia

Available online at www.sciencedirect.com
ScienceDirect
Acta Materialia 59 (2011) 6059–6068
Acta MATERIALIA
www.elsevier.com/locate/actamat

Microstructural development during the quenching and partitioning process in a newly designed low-carbon steel

M.J. Santofimia [a,b,*], L. Zhao [a,b], R. Petrov [c,b], C. Kwakernaak [b], W.G. Sloof [b], J. Sietsma [b]

[a] Materials Innovation Institute (M2i), Mekelweg 2, 2628 CD Delft, The Netherlands
[b] Department of Materials Science and Engineering, Delft University of Technology, Mekelweg 2, 2628 CD Delft, The Netherlands
[c] Department of Metallurgy and Materials Science, Ghent University, Technologiepark 903, 9052 Ghent, Belgium

Received 25 March 2011; received in revised form 6 June 2011; accepted 8 June 2011
Available online 11 July 2011

Abstract

This paper presents a detailed characterization of the microstructural development of a new quenching and partitioning (Q&P) steel. Q&P treatments, starting from full austenitization, were applied to the developed steel, leading to microstructures containing volume fractions of retained austenite of up to 0.15. The austenite was distributed as films in between the martensite laths. Analysis demonstrates that, in this material, stabilization of austenite can be achieved at significantly shorter time scales via the Q&P route than is possible via a bainitic isothermal holding. The results showed that the thermal stabilization of austenite during the partitioning step is not necessarily accompanied by a significant expansion of the material. This implies that the process of carbon partitioning from martensite to austenite occurs across low-mobility martensite–austenite interfaces. The amount of martensite formed during the first quench has been quantified. Unlike martensite formed in the final quench, this martensite was found to be tempered during partitioning. Measured volume fractions of retained austenite after different treatments were compared with simulations using model descriptions for carbon partitioning from martensite to austenite. Simulation results confirmed that the carbon partitioning takes place at low-mobility martensite–austenite interfaces.

Keywords: Steels; Microstructure; Phase transformations

1. Introduction

The development of steels containing combinations of martensite and austenite is one of the most promising approaches being explored for the creation of new advanced high-strength steels (AHSS) [1]. Significant additions of elements such as Si retard the formation of carbides and give rise to the carbon enrichment of austenite via partitioning of carbon from supersaturated martensite. This concept lies at the core of the "quenching and partitioning" (Q&P) process [2,3], which consists of a partial martensite formation (quenching step) from a fully [4] or partially [2] austenitic microstructure, followed by an annealing treatment (partitioning step) at the same or higher temperature to promote carbon partitioning from supersaturated martensite to austenite. During the partitioning step austenite is enriched with carbon, thus allowing its stabilization at room temperature. Complete control of the fraction of martensite (strong phase) and the carbon enrichment of austenite is possible and distinguishes the Q&P process from other AHSS routes.

Although carbon partitioning from martensite to austenite is the principle underlying the Q&P concept, the mechanisms governing this process are the subject of some controversy. It has been postulated that carbon partitioning from martensite to austenite is controlled by the constrained carbon equilibrium (CCE) criterion [2]. This

* Corresponding author at: Delft University of Technology, Mekelweg 2, 2628 CD Delft, The Netherlands. Tel.: +31 152788250; fax: +31 152786730.
E-mail address: m.j.santofimianavarro@tudelft.nl (M.J. Santofimia).

1359-6454/$36.00 © 2011 Acta Materialia Inc. Published by Elsevier Ltd. All rights reserved.
doi:10.1016/j.actamat.2011.06.014

implies that the chemical potential of carbon equilibrates across fixed martensite–austenite interfaces. However, this model does not account for the expansion of the material frequently observed during the partitioning step [5]. The possible mechanisms by which such an expansion can occur include the formation of bainite [6] from austenite, the continued growth of the martensite that was formed during the quenching step [7], or the isothermal nucleation and growth of new martensite [8,9]. In cases where partitioning is performed above the martensite start temperature, the third option is considered unlikely and the possible mechanisms that can produce the observed expansion are reduced to either bainite formation or martensite growth.

For steels with compositions similar to low-alloy transformation-induced plasticity (TRIP) steels the expansion observed during the partitioning step can be readily explained by the formation of bainite [6], since TRIP steel compositions are designed to promote the formation of bainite. In spite of this, a substantial amount of the Q&P research reported to date has focused on TRIP chemical compositions [5,6,10–13] for which bainitic transformation almost certainly plays a role.

To date, studies on chemical compositions specifically optimized for Q&P have not been published in detail. Due to the absence of studies of the Q&P process in alloys in which bainite formation is effectively suppressed, the growth of martensite during the partitioning step has neither been confirmed nor disproved. Even if bainite formation is suppressed, it would be difficult to experimentally detect movement of individual martensite–austenite interfaces. Zhong et al. [7] reported an apparent change in curvature of martensite–austenite interfaces in a steel after partitioning at 450 °C, but it was not clear if that curvature change was actually due to martensite growth.

Thermodynamic studies demonstrate that growth of martensite in the partitioning step is physically possible [9] and warrants study of the kinetics involved. If the CCE condition is relaxed and it is assumed that a difference in chemical potential of iron at the interface acts as a driving force for the movement of the interface, the behavior of martensite–austenite interfaces can be simulated [9]. Such predictions reveal that a net growth of martensite is thermodynamically and kinetically possible until both phases reach equilibrium in the assumed absence of carbide precipitation.

The aim of the present study is to arrive at an improved understanding of the mechanisms governing the partitioning process in the absence of bainitic transformation. With this aim a new steel composition has been designed in which the formation of bainite during the application of Q&P heat treatments can be suppressed. Analysis of the microstructure development during the application of Q&P treatments as well as during isothermal holding in the bainitic transformation range has been performed by dilatometry, X-ray diffraction, optical and scanning electron microscopy, electron back-scattering diffraction (EBSD) and electron probe microanalysis (EPMA).

2. Theoretical design of the Q&P steel chemical composition

The first step of this work was the design of a steel in which a microstructure formed by martensite laths separated by thin films of retained austenite was obtained by the application of appropriate Q&P heat treatments. This steel was designed on the basis of the following requirements:

(a) Absence of ferrite and/or pearlite formation during the quenching step.
(b) Retardation or inhibition of bainite formation, in order to minimize possible overlapping of carbon partitioning and formation of bainite.
(c) Retardation or minimization of the precipitation of carbides, which consumes carbon that is then no longer available for carbon enrichment of the austenite.
(d) A sufficiently high carbon content for thermal stabilization of a considerable fraction of retained austenite at room temperature.

The carbon concentration of the alloy was chosen as 0.2 wt.%. Assuming full partitioning of carbon into austenite, and considering that austenite can be stable at room temperature when its carbon content is around 1.2 wt.%, the chosen carbon concentration is expected to lead to a volume fraction of retained austenite of around 0.16. This volume fraction of retained austenite is close to the fractions usually observed in conventional low-alloy TRIP steels [14].

Manganese, nickel and chromium were included in the chemical composition to retard ferrite, pearlite and bainite formation and to decrease the bainite start temperature, as well as to enhance the austenite stability. A silicon content of 1.5 wt.% was used to inhibit carbide precipitation during the partitioning step.

The thermodynamic model of Bhadeshia for the prediction of TTT diagrams [15], widely applied for the design of steels [16–19], was used for the selection of the steel composition studied in this work. The selected chemical composition is displayed in Table 1 and the predicted TTT diagram is shown in Fig. 1. The predicted martensite and bainite start temperatures (Ms and Bs) are 314 and 320 °C, respectively. This indicates that the predicted temperature range for isothermal bainite formation is very narrow, only 6 °C. The predicted incubation times for bainite formation and ferrite/pearlite formation are 500 and 5000 s,

Table 1
Chemical composition of the steel (wt.%).

C	Mn	Ni	Cr	Si
0.204	2.5	1.47	1.01	1.50

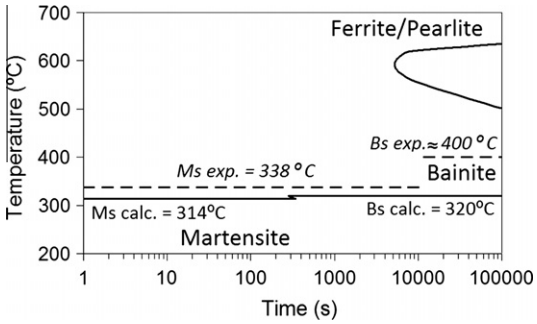

Fig. 1. Prediction of the TTT diagram characteristic of the designed Q&P steel (solid lines) together with experimental values of Ms and Bs temperatures (dashed lines).

respectively. These times suggest that the probability of obtaining ferrite and/or pearlite during cooling is very low in this steel, although formation of bainite during the partitioning step cannot be completely excluded. This fact, together with the reported effect of the martensite transformation promoting the nucleation of bainite [20], justified a detailed experimental analysis of possible formation of bainite during the partitioning step in this steel, which is therefore part of the experimental schedule.

3. Selection and application of heat treatments

The steel was produced using a laboratory vacuum induction furnace. After casting, the steel was hot rolled to a final thickness of 4.5 mm and then air cooled. Cylindrical specimens 4 mm in diameter and 10 mm long were machined parallel to the rolling direction for dilatometry. Heat treatments were applied using a Bähr DIL 805 A/D dilatometer. Four different series of heat treatments (HT) were applied to the specimens, all starting from a full austenitization treatment at 900 °C for 600 s, as shown in Fig. 2.

3.1. Direct quench (HT1, see Fig. 2a)

Treatment consisting of a direct cooling at 50 °C s^{-1} after austenitization. Optical microscopy on the formed microstructure showed only martensite. The absence of bainite and ferrite was also confirmed by the corresponding dilatometry curve. Therefore, a cooling rate of 50 °C s^{-1} was selected as an appropriate cooling rate for the formation of martensite in the quenching step in the subsequent experiments. The measured martensite start temperature (Ms) was 338 °C, which is slightly higher than the value predicted by the model in Fig. 1 (314 °C).

3.2. Bainite treatments (HT2, see Fig. 2b)

Treatments consisting of austenitization followed by cooling at 50 °C s^{-1} to 350, 400 and 450 °C and isothermal holding for times ranging from 10 to 16,000 s. The temperatures were chosen to evaluate the possible formation of bainite within the range of interest for partitioning. These treatments are not Q&P treatments, since they do not include a quenching step below Ms.

3.3. Q&P treatments, partitioning time and temperature dependence (HT3, see Fig. 2c)

Q&P treatments were applied, starting with full austenitization, followed by cooling at 50 °C s^{-1} to a quenching temperature of 275 °C, isothermal holding at that temperature for 5 s and then heating at 10 °C s^{-1} to partitioning temperatures of 350, 400 and 450 °C for times ranging from 3 to 2000 s. The effect of the partitioning step on the microstructure of the steel is evaluated with these treatments.

3.4. Q&P treatments, quenching temperature dependence (HT4, see Fig. 2d)

Q&P treatments were applied, starting with full austenitization, followed by cooling at 50 °C s^{-1} to quenching temperatures ranging from 130 to 316 °C, isothermal holding for 5 s, and then partitioning at 400 °C for 100 s. In this case, the effect of the quenching step is studied under fixed partitioning conditions.

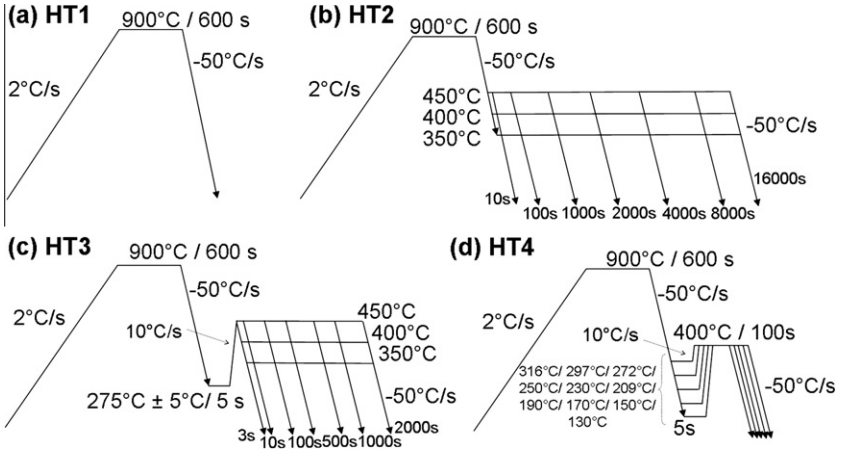

Fig. 2. Heat treatments applied to the steel: (a) HT1 to establish the required quenching rate; (b) HT2 to investigate bainite formation; (c) HT3 to investigate the dependence on partitioning conditions; (d) HT4 to investigate the dependence on quenching temperature.

4. Procedures for microstructural characterization

Heat-treated specimens were cut in half to analyze the surface transverse to the rolling direction. After conventional metallographic preparation, specimens were etched with 2% nital for subsequent optical microscopy and scanning electron microscopy (SEM). SEM observations were performed using a JEOL JSM-6500F field emission gun scanning electron microscope (FEG-SEM) operating at 15 kV.

Specific regions were selected using the FEG-SEM for further study of the alloying element distribution by EPMA. EPMA measurements were performed with a JEOL JXA 8900R microprobe using a 10 keV electron beam with beam current of 50 nA employing wavelength-dispersive spectrometry (WDS). The composition at each analysis location of the sample was determined from the X-ray intensities of the constituent elements after background correction relative to the corresponding intensities of reference materials. The thus-obtained intensity ratios were processed with the matrix correction program CITZAF [21]. An in situ air jet was used to decontaminate the sample surface and to prevent the deposition of carbonaceous substances. The points of analysis were located along a line at intervals of 0.5 μm and carbon, silicon, manganese, chromium, nickel and iron concentrations were determined.

In order to determine the volume fraction of retained austenite in the specimens, X-ray diffraction experiments were performed using a Bruker type D8-Advance diffractometer equipped with a Bruker Vantec Position Sensitive Detector (PSD). Co Kα radiation was used and a 2θ range from 30° to 135°, containing the (1 1 1), (2 0 0), (2 2 0) and (3 1 1) austenite reflections, was scanned using a step size of 0.05°. Error bars in calculations of the volume fraction of retained austenite were estimated to account for possible deviations caused by crystallographic texture. The austenite lattice parameter a_γ was determined from the positions of the maximum of the four austenite reflections using Cohen's method [22]. The carbon concentration x_C of the austenite was obtained using [23,24]:

$$a_\gamma = 0.3556 + 0.00453x_C + 0.000095x_{Mn} + 0.00056x_{Al} + 0.0006x_{Cr} - 0.0002x_{Ni}, \quad (1)$$

where a_γ is the austenite lattice parameter, in nm, and x_C, x_{Mn}, x_{Al}, x_{Cr} and x_{Ni} are the concentrations of carbon, manganese, aluminum, chromium and nickel, respectively, in wt.%. The effect of silicon on the austenite lattice parameter has not been found in the literature and is therefore not included in Eq. (1). The results of this calculation indicate the average value of carbon content in austenite, and do not reveal information on gradients or variations between austenite grains. An error bar of ±0.05 wt.% was estimated for the determination of the carbon content in austenite.

Selected specimens were metallographically prepared for EBSD examination with a final polishing step of 0.05 μm using an OPS suspension. The last specimen preparation step was electrolytic polishing with an electrolyte consisting of 78 ml perchloric acid, 90 ml distilled water, 730 ml ethanol and 100 ml 2-butoxyethanol at 40 V for 10 s. Specimens were analyzed by orientation imaging microscopy (OIM) on a FEI Nova 600 Nanolab dual-beam (focused ion beam) electron microscope equipped with a FEG column. The analysis was performed under the following conditions: acceleration voltage, 20 kV; working distance, 7 mm; tilt angle, 70°; step size, 20 nm. The orientation data were post-processed with Channel 5 software provided by Oxford-HKL®.

5. Results and discussion

In this section, experimental results obtained after application of heat treatments HT2 (bainite treatments), HT3 (Q&P treatments, partitioning dependence) and HT4 (Q&P treatments, quenching dependence) are presented, compared and discussed in Sections 5.1–5.3, respectively. Observed microstructural features lead to the identification of the martensite formed in the first quench of the Q&P treatments in Section 5.4. Finally, experimental results are compared with simulations in Section 5.5.

5.1. Analysis of bainite formation during isothermal holding after full austenitization

Bainite formation in this steel was studied by application of the HT2 heat treatments shown in Fig. 2b. Bainite was observed in the microstructures after full austenitization followed by an isothermal holding at 350 °C. As an example, Fig. 3a shows that the microstructure formed after 4000 s at 350 °C comprises bainite surrounded by martensite. An isothermal hold at 400 °C for 16,000 s and subsequent quenching (Fig. 3b) led to formation of a martensitic microstructure with a small fraction of ferrite grains (volume fraction less than 0.01). Such ferrite grains have not been observed after shorter times. Consideration of the micrographs alone does not reveal whether these ferrite grains are bainitic or allotriomorphic in nature. However, quenching after isothermal holding at 450 °C for 16,000 s results in a fully martensitic microstructure (Fig. 3c) that does not contain any bainite. This strongly suggests that the ferrite formed at 400 °C is bainitic.

These observations indicate that the kinetics of austenite decomposition at 400 and 450 °C is hardly significant after annealing for as long as 16,000 s, in agreement with the predicted TTT diagram of Fig. 1. This makes the experimental determination of the Bs temperature very difficult. However, we can be confident that, on a time scale shorter than around 16,000 s, the maximum estimate for the temperature range for bainite transformation in this steel is between 338 °C (the Ms temperature as measured in the dilatometer) and 400 °C. This temperature range is wider than the range predicted in Fig. 1, but still leaves a signif-

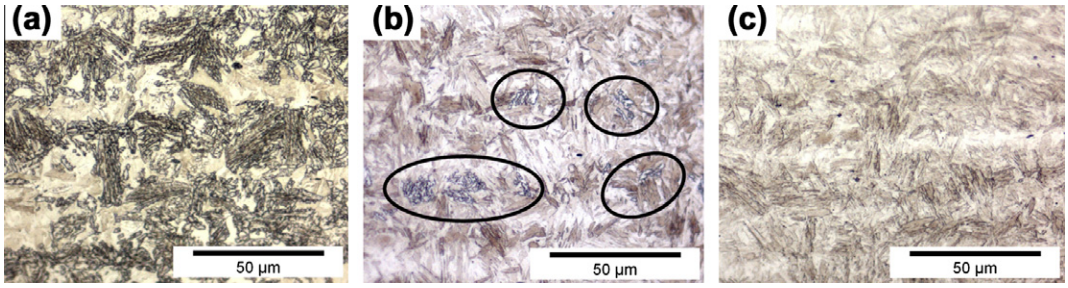

Fig. 3. Light optical micrographs of the steel after HT2 treatments consisting of austenitization at 900 °C for 600 s, cooling at 50 °C s^{-1} and isothermal holding at (a) 350 °C for 4000 s; (b) 400 °C for 16,000 s, and (c) 450 °C for 16,000 s. Circles in (b) indicate zones with isolated ferrite. The specimens were etched with 2% nital.

icant temperature and time window free of isothermal decomposition of austenite into bainite.

Figs. 4 and 5 show the change in length vs. time as measured by dilatometry (Fig. 4) and the measurements of volume fraction and carbon content of retained austenite (Fig. 5) after application of heat treatments HT2 and HT3. Results for HT3 heat treatments will be discussed in Section 5.2. Fig. 4a shows the change in length observed during isothermal holding at 350, 400 and 450 °C. At 350 °C, the observed change in length corresponds to the formation of bainite, as confirmed by the metallographic analysis. On the other hand, at 400 and 450 °C, the expansion was much less (volume changes less than 0.05%), indicating very slow kinetics for austenite decomposition, which was also corroborated by metallographic analysis. In any case, dilatometry shows that the end of the austenite decomposition is not fully reached in the time scale used in the experiments.

Application of HT2 treatments for isothermal treatments at 400 and 450 °C did not lead to the detection of retained austenite after isothermal holdings as long as 16,000 s. In the case of the isothermal holding at 350 °C (Fig. 5a), retained austenite was detected, reaching a volume fraction of 0.02 after holding for 2000 s. In this case, austenite peaks in the diffraction pattern were not strong enough to allow a reliable determination of carbon content in austenite. The analysis indicates that bainite formation is not an effective method for stabilizing significant volume fractions of austenite in this alloy at time scales relevant to continuous production technologies.

5.2. Microstructural evolution during Q&P treatments: different partitioning conditions

In order to determining the effect of partitioning parameters for a fixed quenching temperature (heat treatment series HT3), the target quenching temperature was set to 275 °C, followed by an isothermal holding for 5 s; however, a detailed analysis of the recorded data reveals that the actual quenching temperatures achieved vary in the range 275 ± 5 °C. Dilatometry curves corresponding to the partitioning step at 350, 400 and 450 °C for 2000 s show expansions of 0.06%, 0.03% and 0.02%, respectively (Fig. 4b). Excluding the effect of carbon partitioning on the lattice parameter, the experimentally observed expansions can be associated with formation of volume fractions of body-centered cubic (bcc) phase equal to approximately 0.04, 0.02 and 0.01, respectively.

These expansions cannot be associated with nucleation and growth of martensite, since they occurred at temperatures above Ms. As a consequence, they are likely to be related to the formation of bainite or to isothermal growth of martensite. As discussed in Section 5.1, bainite was observed in micrographs after isothermal treatment at 350 and 400 °C, although at the latter temperature only after extremely long times. Therefore, it is concluded that at 400 and 450 °C, formation of bainite will not take place during the partitioning step applied in HT3. The very slight expansions observed at these temperatures appear therefore to be associated with the isothermal growth of martensite.

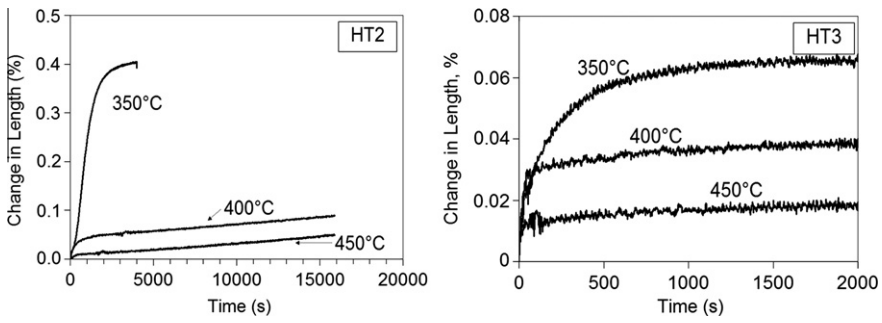

Fig. 4. (a) Dilatation vs. isothermal holding time at 350 °C (4000 s), 400 °C (16,000 s) and 450 °C (16,000 s) in HT2 treatments. (b) Dilatation vs. isothermal holding time at 350 °C (2000 s), 400 °C (2000 s) and 450 °C (2000 s) in HT3 treatments.

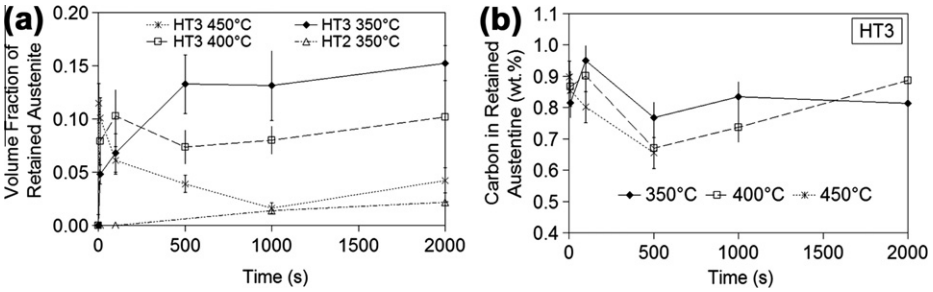

Fig. 5. (a) Volume fractions of retained austenite after HT2 (only 350 °C) and HT3 treatments. (b) Carbon content in retained austenite after HT3 treatment.

Volume fractions of retained austenite obtained after quenching and partitioning at 350, 400 and 450 °C for different partitioning times are presented in Fig. 5a, and corresponding carbon contents are shown in Fig. 5b. After partitioning at 350 °C, the fraction of austenite continuously increases with partitioning time up to a maximum of around 0.15 after partitioning for 2000 s. The average carbon content of the retained austenite reaches a maximum after partitioning for 100 s and, in general, values fall between 0.75 and 0.95 wt.%.

When the partitioning step takes place at 400 °C, the volume fraction of retained austenite reaches a maximum equal to 0.10 after 100 s and remains approximately constant for further increase in partitioning times. The trend is similar to that observed at 350 °C.

In the case of partitioning at 450 °C a maximum in the retained austenite fraction of approximately 0.12 is observed after partitioning for only 3 s. Thereafter a gradual decrease is observed until the partitioning time is equal to 500 s, beyond which the volume fraction of retained austenite remains approximately constant with further increase in time. Austenite diffraction peaks corresponding to partitioning at 450 °C for 1000 and 2000 s were not strong enough to permit a reliable determination of carbon content of retained austenite.

It is clear that the maximum in the volume fraction of retained austenite is reached at shorter times for higher partitioning temperatures, which is in agreement with the expected kinetics of carbon partitioning [9]. For most temperature and time conditions, fractions of retained austenite obtained by the applied Q&P processes are considerably higher and occur at much shorter treatment times than those obtained by cooling directly to an isothermal hold in the bainitic transformation range (HT2). Dilatometry results shown in Fig. 4b indicate that, if bainite is formed during the partitioning step in HT3 treatments, its volume fraction would be too low to explain the observed fractions of retained austenite. Therefore, it is confirmed that, in this steel, the Q&P process is significantly more effective than a bainitic isothermal treatment for the stabilization of austenite.

Microstructures of specimens partitioned at 350, 400 and 450 °C for 1000 s are compared in Fig. 6. The three microstructures look quite similar, consisting of martensite that has responded in two different ways to etching with 2% nital: some laths of martensite are clearly more strongly etched than others. In these micrographs, retained austenite cannot be distinguished from martensite. No significant carbide precipitation is resolved under the electron microscope for any of the samples, indicating that the level of silicon addition is sufficient to inhibit carbide formation.

The morphology of the microstructure present in these materials was further studied by EBSD. Fig. 7 shows an EBSD analysis of the specimen after partitioning at 450 °C for 10 s. Fig. 7a shows a combined band contrast map and color-coded phase map in which blue corresponds to bcc lattice (martensite) and red corresponds to face-centered cubic (fcc) lattice (austenite). Darker bands correspond to a low band contrast. Retained austenite is distributed both as small films of around 200 nm thickness and 1–2 μm in length and as grains of nanometer size (which is at the limit of the instrumental resolution) between martensite laths. Most of the austenite grains are located between martensite laths with higher band contrast and larger size. This observation suggests that martensite with higher band contrast and larger size was formed during the first quenching step and underwent partitioning of carbon to the surrounding austenite, contributing to its thermal stabilization, whereas martensite with lower band contrast was formed in the last quench. Fig. 7b shows a combined band-contrast map and inverse pole-figure map of the austenite grains. This figure shows that austenite grains situated in the same region share the same crystallographic orientation. These austenite grains probably originate from a single prior austenite grain.

5.3. Microstructural evolution after Q&P treatments with variable quenching conditions and partitioning at 400°C for 100 s

As was shown in Section 5.2, for a quenching temperature of 275 ± 5 °C, a local maximum in the volume fraction of retained austenite, is observed after application of a partitioning step at 400 °C for 100 s in the absence of bainitic transformation. In the heat treatment series HT4, these partitioning conditions of 100 s at 400 °C were applied after quenching to different temperatures.

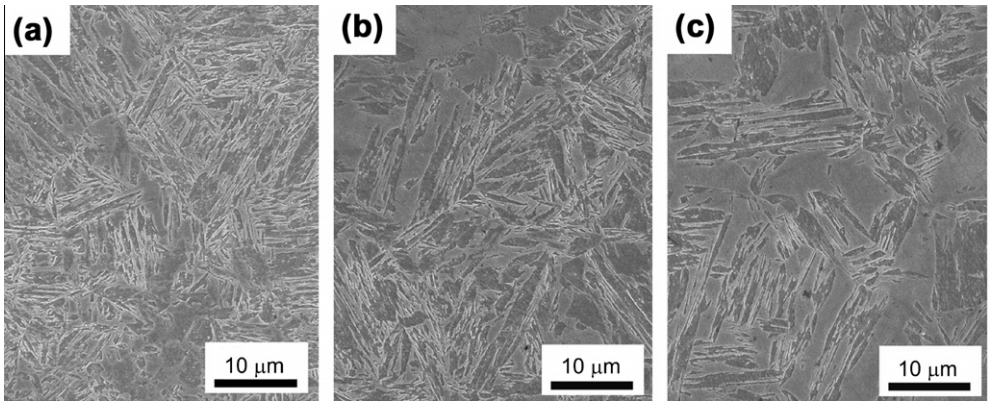

Fig. 6. Scanning electron micrographs of the steel after full austenitization, quenching to 275 °C ± 5 °C and partitioning for 1000 s at: (a) 350 °C, (b) 400 °C, and (c) 450 °C. The specimens were etched with 2% nital.

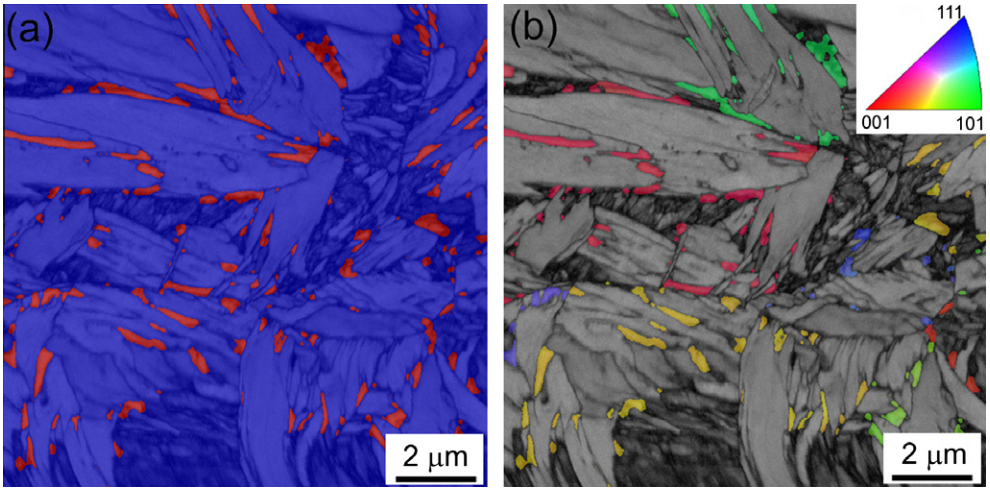

Fig. 7. EBSD analysis of the microstructure obtained after full austenitization, quenching to 275 ± 5 °C and partitioning at 450 °C for 10 s.

Fig. 8 shows the measurements of volume fraction and carbon content of retained austenite as a function of the quenching temperature. The average carbon content of the retained austenite ranges from 0.8 to 1.0 wt.% and appears to be almost independent of the quenching temperature. However, a distinct maximum in the volume fraction of retained austenite is observed for a quenching temperature of 230 °C. If the partitioning of carbon is assumed to be complete after 100 s at 400 °C [9], a hypothetical explanation for this observation can be offered [2]. A lower quenching temperature results in the formation of a higher fraction of martensite in the first quench and consequently implies that a lower austenite fraction of austenite will be available for stabilization. On the other hand, after quenching to a higher temperature, the martensite fraction available to transfer carbon to austenite is lower, potentially leading to a high fraction of relatively unstable austenite that transforms to martensite in the final quench. The compromise between the two situations can be envisaged to lead to a maximum in the volume fraction of retained austenite as a function of quenching temperature, which in the case of this material is found at around 230 °C.

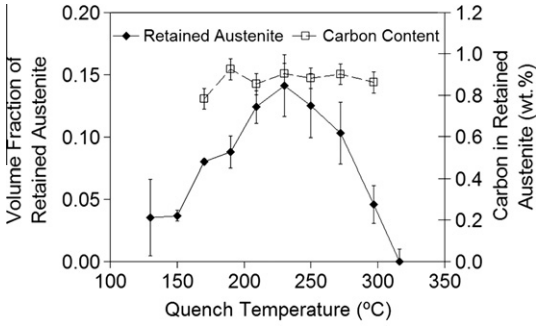

Fig. 8. Volume fraction of retained austenite and corresponding carbon content after full austenitization, quenching to different temperatures and partitioning at 400 °C for 100 s (heat treatment HT4).

5.4. Characterization of the martensite formed in the first quench of the Q&P process

It is interesting to further investigate the effect that the partitioning step has on the martensite formed in the first quench. EBSD results reveal two types of martensite and it is suggested that the martensite with a higher band contrast and larger size was formed during the quenching step

and has released its carbon to the surrounding austenite during the partitioning step. The same martensite grains were observed in FEG-SEM images to be differently etched by 2% nital, According to these observations, martensite with higher band contrast and larger size can be expected to contain less carbon than the rest of the microstructure. To provide confirmation, EPMA analyses were performed on the HT3 specimen partitioned at 450 °C for 1000 s. The results are shown in Fig. 9. Fig. 9a shows a FEG-SEM image of the specimen, where the arrow indicates the line along which the EPMA analysis was performed. Fig. 9b and c shows the observed carbon and substitutional-element compositions. The heavier etched areas in the microstructure contained less carbon than the lightly etched ones. The substitutional alloying elements concentrations are constant, independent of the position with respect to an interface separating grains of the two types of martensite. These observations strongly suggest that the heavily etched martensitic regions correspond to martensite formed in the first quench (subsequently referred to as M_1), whereas the rest of the microstructure consists of martensite formed in the final quench and retained austenite. The absence of any significant dilatation during partitioning at 400 and 450 °C implies that these etched laths correspond to martensite and not to another bcc phase such as bainite. Similar conclusions were recently presented by Wang et al. [25]. Due to compositional differences between M_1 and the martensite formed in the final quench of the Q&P process, variations in the volume fraction of M_1 can lead, in principle, to changes in the mechanical properties of the material. This observation demonstrates the importance of a good control of the quenching temperature.

The volume fraction of the martensite laths that underwent strong etching with 2% nital were measured for all available specimens, including specimens described in the previous section, from FEG-SEM pictures, except the ones corresponding to partitioning at 350 °C, in which the observed dilatation during the partitioning step could be associated to bainite formation. According to the EPMA observations, these martensite laths correspond to M_1. The results, presented in Fig. 10 as a function of the quenching temperature, show that the volume fraction of M_1 decreases with increasing quenching temperature. Error bars represent the standard deviation of the measurements. Values for the volume fraction of M_1 have been normalized to 0.96 because a volume fraction of retained austenite equal to 0.04 was measured in the specimen obtained after application of a direct quench (HT1). The multiple data points plotted at temperatures around 275 °C reveal that the scatter observed in the quenching temperature in the HT3 series of heat treatments (±5 °C) led to a scatter in the resulting volume fraction of M_1.

Measurements of the volume fraction of M_1 were fitted to the Koistinen–Marburger equation [26]:

$$v_{M1} = 1 - \exp(-\alpha_m \cdot (T_{KM} - T_Q)), \quad (2)$$

where α_m is the rate parameter, T_{KM} the so-called theoretical martensite start temperature (which can be somewhat lower than Ms [27]), v_{M1} is the calculated volume fraction of M_1, and T_Q is the quenching temperature. The fit yields values of $\alpha_m = 0.01824\ \mathrm{K}^{-1}$ and $T_{KM} = 325$ °C. A line representing this fit is shown in Fig. 10. It is interesting to point out that obtained values for fitting parameters are in agreement with the ones obtained for the compositional dependence of α_m and T_{KM} proposed by Van Bohemen et al. [27] ($0.01827\ \mathrm{K}^{-1}$ and 304 °C, respectively), which include all alloying elements present in the steel except silicon.

5.5. Prediction of volume fractions of retained austenite after Q&P treatments and comparison with experimental results

The inhibition of bainite in HT3 treatments when partitioning occurs at 400 and 450 °C makes the experimental results observed on those specimens suitable for comparison with simulations performed using the model of the kinetics of carbon partitioning from martensite to austenite presented in Refs. [9,28]. Applying the method presented in Ref. [29], calculated carbon profiles were also converted into volume fractions of retained austenite for comparison with experimental data.

Simulations were performed assuming a binary Fe–0.20 wt.% C system and an assumed martensite–austenite film morphology. The volume fractions of M_1 calculated from Eq. (2) as a function of the experimental quenching temperature were used as input values of the volume fraction of martensite prior to the partitioning step. Initial

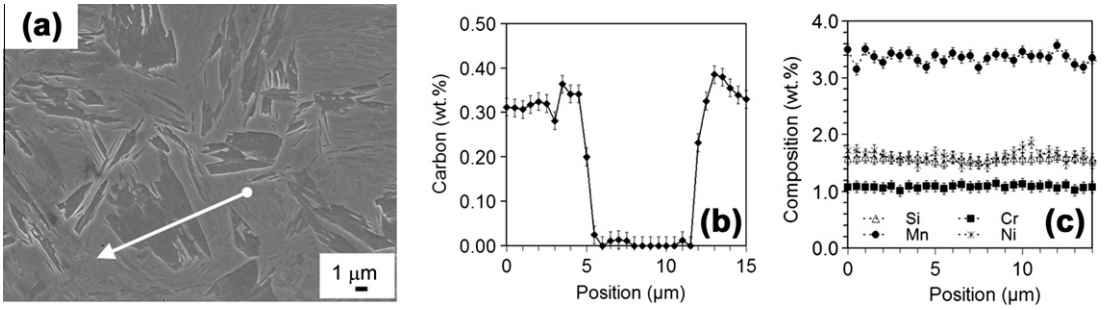

Fig. 9. EPMA analysis of the steel after full austenitization, quenching at 275 ± 5 °C and partitioning at 450 °C for 1000 s.

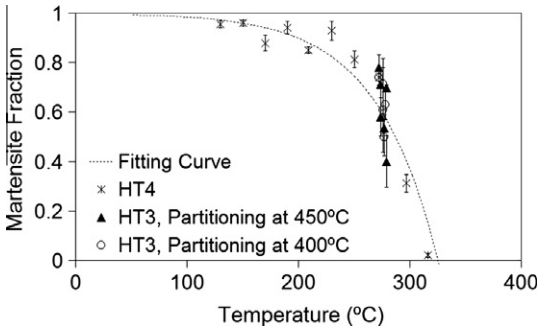

Fig. 10. Volume fraction of martensite formed during first quench vs. quenching temperature, fitted by Eq. (2).

volume fractions of phases prior to the partitioning step were converted into lath widths of martensite and austenite according to the method presented in Ref. [30].

In the present work, a low martensite–austenite interface mobility corresponding to the activation energy for the migration of iron atoms across the interface of 215 kJ mol^{-1} was adopted for the simulations. This mobility is in agreement with the small expansion that was experimentally observed during partitioning at 400 and 450 °C for 2000 s (Fig. 4b). A comparison of experimentally determined volume fractions of retained austenite with values calculated from simulations is presented in Fig. 11. Fig. 11a presents the results corresponding to the HT4 heat treatments, in which quenching temperatures were varied for constant partitioning conditions (400 °C, 100 s). For all quenching temperatures other than 230 and 250 °C the simulated phase fractions reproduce the experimental values within experimental accuracy. This shows that the activation energy of 215 kJ mol^{-1}, which implies a low mobility of martensite–austenite interfaces, is a good approximation for the interface kinetics related to carbon partitioning from martensite to austenite.

Simulated and measured volume fractions of retained austenite after partitioning at 400 and 450 °C for different partitioning times are presented in Fig. 11b and c. The simulated data reproduce the trends observed in the experimental data. Part of the difference between the experimental and simulated values can be attributed to the use of Eq. (2) in the determination of the input values for v_{M1} for quenching temperatures close to 275 °C. Although Eq. (2) describes the martensite formed in the first quench of the Q&P process with high accuracy, actual volume fractions can be slightly different from the predicted ones for cases in which the aimed quench temperature of 275 °C was not achieved in practice (Fig. 10). The observed variation in both the experimental and simulated retained austenite volume fractions with partitioning time will reflect not only the effect of the carbon partitioning, but also the effect of variation in the fraction of M_1. Consider, for example, partitioning at 450 °C for 500 and 1000 s. Although an increase in the fraction austenite with increasing partitioning time may be expected, from Fig. 11c it is apparent that both the measured and predicted values

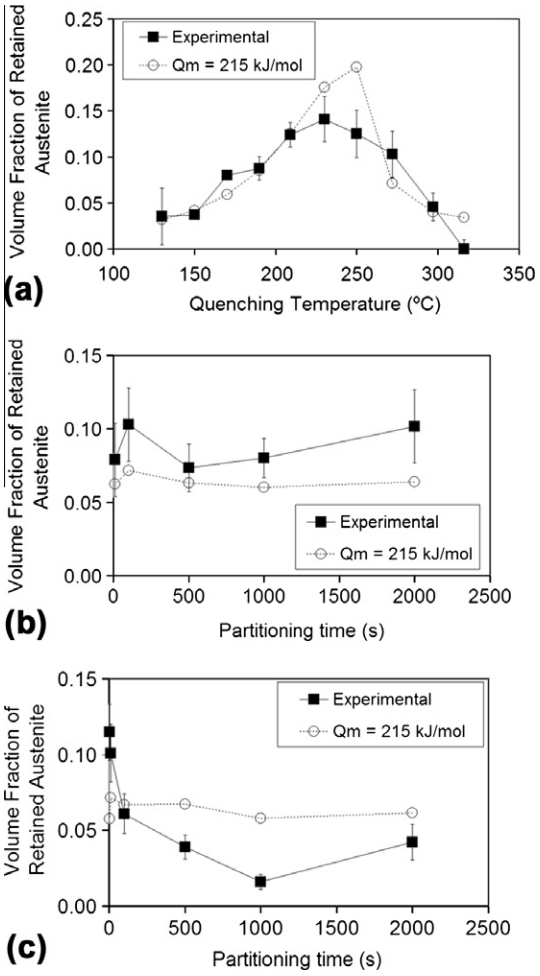

Fig. 11. Comparison between experimental and calculated values of volume fractions of retained austenite: (a) treatment HT4; (b and c) treatment HT3 with partitioning at (b) 400 °C and (c) 450 °C.

of retained austenite volume fraction after partitioning for 500 s are higher than those after partitioning for 1000 s. However, at this temperature, the process of carbon partitioning is practically complete after 100 s and simulations show that the decrease in the volume fraction retained austenite is due to the small variations in the actual quenching temperature achieved. The dependences of volume fraction of retained austenite and martensite formed in the first quench with quenching temperature illustrate the importance of a good control of the process parameters in the application of the Q&P process.

6. Conclusion

A design procedure for the development of Q&P steels was successfully applied for the creation of a new optimized Q&P chemical composition. Application of appropriate Q&P processing variations to this steel led to microstructures comprising martensite and films of retained austenite (the latter up to a volume fraction of 0.15), embedded in the martensite microstructure. Martensite formed in the first quench has been identified as well

as quantified in the microstructures. For the chemical composition studied, at time scales relevant to commercial continuous processes, considerably higher volume fractions of metastable retained austenite can be achieved via Q&P than via a bainitic holding. Results also reveal that the thermal stabilization of austenite during partitioning is not necessarily accompanied by a significant volume expansion. Following this observation, simulations of the kinetics of carbon partitioning from martensite to austenite were performed assuming a low-mobility martensite–austenite interface. These simulations accurately reproduce the experimentally measured volume fractions of retained austenite, suggesting that martensite–austenite interfaces move only slightly during the process of carbon partitioning from martensite to austenite for the alloy composition and conditions of temperature and time evaluated in this work.

Acknowledgements

This research was carried out under the project number M41.09246 in the framework of the Research Program of the Materials innovation institute M2i (www.m2i.nl). The support of TATA Steel RD&T to this project is acknowledged. In particular, the authors would like to express their gratitude to Dr. Filippo Zuliani for fruitful discussions and to Dr. David N. Hanlon for his valuable contribution in the editing of this manuscript.

References

[1] Matlock DK, Speer JG. Third generation of AHSS: microstructure design concepts. In: Microstructure and texture in steels. London: Springer; 2009. p. 185–205.
[2] Speer JG, Streicher AM, Matlock DK, Rizzo FC, Krauss G. In: Damm EB, Merwin M, editors. Austenite formation and decomposition. Warrendale, PA: TMS/ISS; 2003. p. 505–22.
[3] Speer JG, Matlock DK, Edmonds DV. Mater Res 2005;8:417.
[4] Matlock DK, Bräutigam VE, Speer JG. Mater Sci Forum 2003;426–432:1089.
[5] Kim SJ, Kim HS, De Cooman BC. In: Proc mater sci technol, Detroit, MI, MS&T; 2007. p. 73–83.
[6] Santofimia MJ, Zhao L, Sietsma J. Metall Mater Trans A 2009;40A:46.
[7] Zhong N, Wang X, Rong Y, Wang L. J Mater Sci Technol 2006;22:751.
[8] Kim SJ, Speer JG, Kim HS, De Cooman BC. In: International conference on new developments in advanced high-strength steels, AIST, Orlando, FL; 2008. p. 179–89.
[9] Santofimia MJ, Speer JG, Clarke AJ, Zhao L, Sietsma J. Acta Mater 2009;57:4548.
[10] Santofimia MJ, Zhao L, Sietsma J. Mater Charact 2008;59:1758.
[11] Jin JW, Byun SH, Lee SB, Kim SI, Oh CS, Kang N, et al. In: International conference on new developments in advanced high-strength steels, AIST, Orlando, FL; 2008. p. 169–78.
[12] Streicher AM, Speer JG, Matlock DK, De Cooman BC. In: Speer JG, editor. International conference on advanced high strength sheet steels for automotive applications, AIST, Warrendale, PA; 2004. p. 51–62.
[13] Zhong N, Wang XD, Huang BX, Rong YH, Wang L. In: International conference on advanced structural steels, Gyeongju, Korea; 2006. p. 885–91.
[14] De Cooman BC. Curr Opin Solid State Mater Sci 2004;8:285.
[15] Bhadeshia HKDH. Metal Sci 1981;15:178.
[16] Caballero FG, Santofimia MJ, Capdevila C, Garcia-Mateo C, Garcia de Andres C. ISIJ Int 2006;46:1479.
[17] Santofimia MJ. PhD thesis, Universidad Complutense de Madrid; 2006.
[18] Caballero FG, Bhadeshia HKDH, Mawella KJA, Jones DG, Brown P. Mater Sci Technol 2001;17:512.
[19] Santofimia MJ, Nguyen-Minh T, Zhao L, Petrov R, Sabirov I, Sietsma J. Mater Sci Eng A 2010;527:6429.
[20] Kawata H, Hayashi K, Sugiura N, Yoshinaga N, Takahashi M. Mater Sci Forum 2010;638–642:3307.
[21] Armstrong JT. In: Heinrich KFJ, Newbury DE, editors. Electron probe quantization. New York: Plenum Press; 1991. p. 261–315.
[22] Cullity BD. Elements of X-ray diffraction. Reading, MA: Addison-Wesley; 1978. p. 359–67.
[23] van Dijk NH, Butt AM, Zhao L, Sietsma J, Offerman SE, Wright JP, et al. Acta Mater 2005;53:5439.
[24] Dyson DJ, Holmes B. J Iron Steel Inst 1970;208:469.
[25] Wang CY, Shi J, Cao WQ, Dong H. Mater Sci Eng A 2010;527:3442.
[26] Koistinen DP, Marburger RE. Acta Metall 1959;7:59.
[27] van Bohemen SMC, Sietsma J. Metall Mater Trans A 2009;40A:1059.
[28] Santofimia MJ, Zhao L, Sietsma J. Scripta Mater 2008;59:159.
[29] Clarke AJ, Speer JG, Matlock DK, Rizzo FC, Edmonds DV, Santofimia MJ. Scripta Mater 2009;61:149.
[30] Clarke AJ. PhD thesis, Colorado School of Mines; 2006. p. 31–32.